SCIENTIFIC Publishing Limited

Neurolinguistic Communication Intervention

https://ojs.ukscip.com/index.php/nci

Article

Characterizing Language Network Connectivity Changes in Autism Spectrum Disorder Using Graph Theory and Machine Learning: A Multisite Functional Magnetic Resonance Imaging Study

Huibin Ma[a, 1] | Jinying Wu[a, 1] | Lanfen Chen[b, 1] | Jiaying Song[a] | Hang Zhang[b] | Zeqi Hao[c] | Linlin Zhan[d] | Lulu Cheng[e, *] | Xize Jia[c, f, *]

a School of Information and Electronics Technology, Jiamusi University, Jiamusi, 154007, China
b School of Medical Imaging, Shandong Second Medical University, Weifang, 261053, China
c School of Psychology, Zhejiang Normal University, Jinhua, 321004, China
d Faculty of Western Languages, Heilongjiang University, Harbin, 150080, China
e School of Foreign Studies, China University of Petroleum (East China), Qingdao, 266580, China
f Intelligent Laboratory of Zhejiang Province in Mental Health and Crisis Intervention for Children and Adolescents, Zhejiang Normal University, Jinhua, 321004, China

ABSTRACT

Autism spectrum disorder (ASD) is associated with atypical language-related functional connectivity (FC), though network-level substrates of verbal ability across large multisite cohorts require further characterization. In this study, resting-state fMRI data from 219 individuals with ASD and 322 healthy controls with valid verbal IQ (VIQ) scores were obtained from 12 sites in the ABIDE database. ROI-based FC and whole-brain network metrics were computed and correlated with VIQ. Three feature sets—raw connectivity and topology, group-difference metrics, and metrics combined with VIQ—were evaluated using SVM and manifold learning. ASD participants showed widespread FC alterations with overall increases and selective decreases in specific networks. At the global level, ASD patients exhibited a significantly lower AUC specifically for the normalized clustering coefficient γ ($p < 0.05$), while other metrics showed no significant group differences. Nodal analyses revealed increased degree centrality and efficiency in subcortical and frontal regions and reductions in limbic and temporal areas (all $p < 0.05$). Anterior cingulate centrality correlated negatively with VIQ, while occipital metrics correlated positively. The classification reached a peak AUC of 0.7514, which is competitive for large-scale multisite analysis and demonstrates the relevance of VIQ-related features in a proof-of-principle context. These results provide a proof-of-principle for the relevance of VIQ-related network features. These findings suggest that aberrant FC linked to verbal ability reflects key aspects of ASD pathophysiology, emphasizing the importance of integrating behavioral scales into neuroimaging research.

Keywords: autism spectrum disorder; functional connectivity; manifold dimensionality reduction; machine learning; graph theoretical analysis; language network

1. Introduction

Autism spectrum disorder (ASD) is a neurodevelopmental condition characterized by impairments in social communication, the presence of restricted interests, and repetitive or stereotyped behaviors (Association, 2013). Language impairment is a prominent feature of ASD, manifesting as pragmatic deficits, and reduced communicative functions (Márquez-García et al., 2023) , as well as difficulty integrating contextual cues during language process (Vulchanova et al., 2015). All these are intrinsically linked to core social communication difficulties (Gibson et al., 2013; Kjelgaard et al., 2001; Larson et al., 2022; Riches et al., 2010) and can profoundly affect the learning ability, even blocking communication with the outside world. However, the underlying neurofunctional mechanisms associated with these language impairments in ASD remain incompletely understood.

Recently, functional magnetic resonance imaging (fMRI), with its high temporal and spatial resolution and non-invasive nature (Dichter, 2012; Goense et al., 2016) has become a pivotal tool for probing the neural mechanisms of diseases, and the aberrant brain network connectivity in ASD has been paid extensive attention(Lin et al., 2024). For instance, Bi et al. (Bi, Zhao, et al., 2018) reported that ASD patients exhibit decreased functional connectivity (FC) in the default mode (DMN), central executive (CEN), cerebellar (CN), visual (VN), salience (SRN) and dorsal attention (DAN) networks, alongside increased FC in the auditory (AN) and sensorimotor (SMN) networks. Similarly, Peng et al. (Peng et al., 2022) identified aberrant functional brain network connections in ASD, most notably between the right parahippocampal gyrus (PHG.R) and the left pallidum (PAL.L). Collectively, these findings support the hypothesis that altered FC is a defining feature of ASD (Horien et al., 2022). While, most investigations have been constrained by relatively small sample sizes, limiting generalizability (Larson et al., 2022; Williams et al., 2013; Wu et al., 2025).

However, traditional analyses of FC have primarily focused on regional interactions, making it hard to detect whole-brain FC. Now, researchers have applied graph-theoretical methods to FC (Alaerts et al., 2015; Keown et al., 2017), which enables a more comprehensive examination of both local and global networks in the human brain(van den Heuvel et al., 2010). Graph theory analysis applies mathematical frameworks to represent the brain as a network of nodes (brain regions) and edges (functional connections), allowing quantification of topological properties that go beyond pairwise FC measures (Bressler et al., 2010; Bullmore et al., 2009; Olaf Sporns, 2010; O. Sporns, 2013). Using this approach, researchers have extensively characterized functional brain networks in ASD through global metrics such as average local clustering coefficient (Cp) and characteristic path length (Lp), as well as nodal metrics such as degree and efficiency (Chen et al., 2021; Keown et al., 2017; Rudie et al., 2012). Studies of FC in ASD have further pinpointed how language and attention networks diverge from typical development. For example, Lee et al. (Lee et al., 2017), using the Autism Brain Imaging Data Exchange (ABIDE) cohort, found reduced DC of the left inferior frontal gyrus in children with ASD and of the left posterior superior temporal gyrus in adults, alongside increased DC of the middle temporal gyrus within the language network in adults with ASD relative to neurotypical peers. Analyses of the FC between pairs of networks have also revealed significantly elevated coupling between the DMN and language networks, as well as between VN and VAN in individuals with ASD (Alamdari et al., 2022).

In previous ASD language research, social communication measures, most commonly the Autism Diagnostic Observation Schedule (ADOS), have predominated (Lee et al., 2017; Moraglia et al., 2025), with few studies directly indexing language performance. Existing research has demonstrated that the discrepancy between Verbal Intelligence Quotient (VIQ) and Performance IQ (PIQ) is closely associated with ASD

symptom severity, with VIQ emerging as a critical predictor (Johnson et al., 2021). Given the important role of VIQ in characterizing language deficits in ASD, this study selects VIQ as a clinical indicator of language impairment to examine its associations with FC and graph-theoretical network metrics, thereby shedding light on underlying neuropathological mechanisms.

Additionally, machine learning has become an essential tool for the diagnosis and prediction of neurological disorders (Klöppel et al., 2012; Orrù et al., 2012). Support-vector machine (SVM) is a class of supervised algorithms designed to find the optimal separating hyperplane for classification tasks, typically using voxel-wise or ROI-based signals extracted from fMRI data as features (Pereira et al., 2009). The SVM has been extensively used for classifying various neurological conditions. For example, it has been used to discriminate Parkinson's patients from healthy controls by employing connection weights and network metrics (Li et al., 2023); to classify Alzheimer's disease based on the upper-triangular entries of the connectivity matrix (Li et al., 2020); and to identify ASD using graph-theoretical network metrics—degree, shortest path length, local efficiency (Eloc) and Cp (Bi, Wang, et al., 2018). However, SVM performance can be compromised by the high dimensionality, noise, and redundancy of neuroimaging-derived features (Li et al., 2017), necessitating appropriate feature selection or dimensionality reduction to ensure robust classification. Principal component analysis (PCA) decomposes fMRI time series into orthogonal components, allowing low-variance (noise) components to be removed and thereby enhancing BOLD contrast sensitivity (Thomas et al., 2002). Uniform Manifold Approximation and Projection (UMAP) is a nonlinear manifold-learning technique that projects high-dimensional data into a low-dimensional embedding by jointly optimizing local neighborhood preservation and global topological structure (Casanova et al., 2021; Healy et al., 2024). In the context of fMRI, UMAP has been applied to FC matrices and voxel-wise activation patterns to reveal intrinsic network organization and to distinguish among cognitive or clinical states (Casanova et al., 2021; Healy et al., 2024). Accordingly, we propose two distinct pipelines for identifying FC neuromarkers in ASD: one using manual feature selection for dimensionality reduction followed by SVM classification, and another that performs automated dimensionality reduction through PCA combined with UMAP embedding prior to SVM classification. Both pipelines were evaluated for their diagnostic utility.

In the present study, we leveraged the open-access Autism Brain Imaging Data Exchange (ABIDE; http://fcon_1000.projects.nitrc.org/indi/abide/) repository to address the sample size limitations and to enable assessment of reproducibility across multiple sites (Di Martino et al., 2014). Using multisite ABIDE neuroimaging data, we examined whole-brain FC and graph-theoretical metrics in ASD and VIQ-correlation analyses. Based on these results, we constructed three feature sets—raw connectivity, group-difference connectivity and network metrics, and a VIQ-augmented differential-language set—and evaluated classification performance with SVM. We posited that both manual feature selection and the PCA-UMAP dimensionality reduction pipeline would yield robust discrimination between ASD and controls. Moreover, we hypothesized that embedding VIQ-related network alterations would further boost biomarker sensitivity, and that the integrative use of neuroimaging, graph theory, and machine learning would reveal robust language-related neuromarkers of ASD.

2. Materials and methods

2.1. Participants

We used neuroimaging data from the ABIDE initiative, specifically ABIDE I (http://fcon_1000.projects.nitrc.org/indi/abide/abide_I.html) (Di Martino et al., 2014) and ABIDE II (http://fcon_1000.projects.nitrc.

org/indi/abide/abide_II.html) (Di Martino et al., 2017). The inclusion criteria were as follows: (1) availability of both functional and structural MRI data; (2) successful spatial normalization; (3) minimal head motion artifacts, defined as translational displacement ≤3 mm and rotational movement ≤3°; (4) inclusion of both ASD and healthy controls (HCs) within each cohort; and (5) right-handedness to control for lateralization effects. After applying these criteria, we further selected participants with available and valid VIQ scores, as assessed by the Wechsler Abbreviated Scale of Intelligence (WASI) (Wechsler, 1999). This yielded a final sample of 541 participants, including 219 individuals with ASD and 322 HCs.

Additional information on scanning protocols, ethical approvals, and data acquisition procedures can be found on the ABIDE project website (http://fcon_1000.projects.nitrc.org/indi/abide/).

2.2. Rs-fMRI data preprocessing

All of the functional images were preprocessed using rs-fMRI Data Analysis Toolkit plus (RESTplus V1.28, http://restfmri.net/forum/restplus) (Jia et al., 2019) in MATLAB 2022b (MathWorks, Natick, MA, USA). Specifically, the following steps were conducted: (1)discarding the first 10 time points; (2) slice timing correction; (3)head motion correction; (4) spatial normalization to the Montreal Neurological Institute (MNI) space using deformation fields derived from the new segmentation of structural images, followed by resampling to 3×3×3 mm^3; (5)spatial smoothing with a 4 mm full width at half maximum (FWHM); (6)linear detrending; (7) nuisance signal regression with the Friston-24 head motion parameters as covariate (Friston et al., 1996); (8)bandpass filtering in conventional (0.01–0.08 Hz) bands.

2.3. FC analysis

To construct subject-specific FC matrices, we employed the Automated Anatomical Labeling (AAL90) atlas to define the brain's network architecture. The AAL90 atlas is currently the most popular parcellation scheme in fMRI research and has been widely used to identify a variety of psychological disorders in recent years (Dai et al., 2012; Wee et al., 2012; Zeng et al., 2012). This atlas partitions the brain into 90 anatomically constrained regions of interest (ROIs), resulting in a comprehensive whole-brain parcellation (Tzourio-Mazoyer et al., 2002). For each subject, blood-oxygen-level-dependent (BOLD) signals were extracted from each ROI, and the time series were band-pass filtered to reduce physiological noise. FC between ROI pairs was then quantified by computing Pearson correlation coefficients between their respective time series. The Pearson correlation coefficients were normalized using Fisher-Z transformation to serve as edge weights. The resulting FC matrix was symmetric, with each element representing the strength of temporal coherence between two brain regions.

2.4. Network metrics

To characterize the global topology and regional attributes of brain functional networks across different sparsity thresholds, we constructed weighted networks over a cost range from 0.05 to 0.50 in 0.05 increments and computed both global metrics and regional node parameters using the GRETNA software package (Rubinov et al., 2010; Wang et al., 2015).

The global metrics include (1) small-world properties—Cp, Lp, global clustering coefficient (γ), normalized characteristic path length (λ), and small-worldness (σ)—and (2) network efficiency measures—global efficiency (Eglob) and Eloc. The normalized metrics were derived as γ = Cp/Cprand and λ = Lp/Lprand, where Cprand and Lprand were obtained from random networks.High Cp, γ, and Eloc indicate strong functional segregation, reflecting local interconnectivity within the network. Conversely, low Lp, λ, and high Eglob suggest efficient functional integration, facilitating global information exchange. Small-

worldness quantifies the balance between local specialization and global communication, with small-world networks exhibiting both high global clustering coefficients ($\gamma > 1$) characteristic of regular lattices and short characteristic path lengths ($\lambda \approx 1$) typical of random networks (Watts et al., 1998).

To assess regional node properties, we calculated betweenness centrality (BC), degree centrality (DC), nodal efficiency (NE), and nodal local efficiency (NLE). BC quantifies a node's influence on information flow, with higher values indicating a greater role in communication pathways (Freeman, 1978). DC measures the number of direct connections a node has, reflecting its connectivity (Rubinov et al., 2010). NE evaluates a node's capacity for parallel information transmission, while NLE represents the inverse of the shortest average path length within a node's local subgraph, serving as an indicator of network robustness (Achard et al., 2007).

Because area under the curve (AUC) can select single threshold calculation independently, and is highly sensitive about topology structure of brain disease abnormally, we calculated the AUC for each network metric (Zhang et al., 2011).

2.5. Statistical analysis

All statistical analyses of demographic variables were conducted using SPSS version 27.0 (IBM Corp., Armonk, NY). Specifically, all comparisons were performed separately at each site: two-sample *t*-tests were used to assess group differences in age, while sex distributions were compared using the chi-square (χ^2) test. Statistical significance was determined using a threshold of $p < 0.05$.

To examine group differences in functional brain networks and associated topological metrics between the ASD and HCs, we conducted two-sample t-tests using the GRETNA toolbox (Wang et al., 2015). Statistical significance was determined using false discovery rate (FDR) correction with a threshold of $p < 0.05$, applied to control for multiple comparisons across network measures (Benjamini et al., 1995).

To examine the relationship between brain network features and language ability, we performed Pearson correlation analyses in MATLAB (version 2022a). Specifically, for each subject we extracted (1) the z-values of those FC edges showing group differences between ASD and HCs, and (2) global and nodal graph-theoretical network metrics. These features were then correlated against VIQ scores across all subjects. The correlation strength and significance were quantified by Pearson's r and the corresponding p-values. Statistical significance was defined as $p < 0.05$.

2.6. Manual feature selection

To investigate the impact of feature selection on classification performance, we constructed three 541 × N feature matrices (where rows correspond to participants and columns to features). The raw feature matrix was formed by flattening the upper-triangular entries of each participant's FC matrix into a row vector and concatenating this with the flattened row vector of all computed network metrics. The differential feature matrix was then derived by repeating this procedure only for those FC edges and network metrics that showed significant group differences (FDR, $p < 0.05$). Finally, the differential-language feature matrix was created by appending each participant's VIQ score as an additional column to the differential feature matrix. For all three matrices, a final column of class labels was added (ASD = 1, HCs = 2) before feeding into a classifier with uniform parameter settings.

2.7. Machine learning

All imaging-derived features were first split into training and hold-out test sets by stratified sampling to preserve class proportions, with 80 % of the data used for training and 20 % reserved for final evaluation.

After data splitting, a Min–Max scaler was fit on the training features and applied to both training and test sets to map each feature independently into the [0, 1] interval. Within the training set, we performed ten-fold cross-validation: the training data were randomly shuffled and partitioned into ten equal folds, each maintaining the original distribution of classes. In each fold, two parallel pipelines were executed. In the first pipeline, a support vector machine classifier with a radial basis function kernel was trained directly on the normalized features using fixed hyperparameters determined in preliminary experiments. In the second pipeline, we first reduced feature dimensionality by optionally applying PCA—treating the decision to use PCA and the proportion of variance to retain as parameters to be optimized—followed by UMAP embedding, where the number of neighbors, minimum distance, distance metric, and target dimensionality were likewise tuned. Model selection in both pipelines involved grid search over kernel types and regularization parameters (C and γ), class weights were adjusted to compensate for imbalance, probabilistic outputs were enabled, and all randomization steps were governed by a single seed to ensure full reproducibility. After cross-validation, each pipeline's optimal parameter set was used to retrain a final model on the entire training set, and the discriminative performance of these models was assessed on the hold-out test set by computing the AUC.

3. Results

3.1. Demographic and clinical information

The demographic information of the current study was summarized in Table 1. A total of 2,168 participants were initially included from ABIDE I and ABIDE II datasets. After applying inclusion criteria, 228 individuals were removed due to excessive head motion (exceeding 3 mm or 3°), 213 due to poor normalization quality, 14 for missing usable functional images, and 16 for missing structural images. A further 55 participants were excluded due to a lack of HCs. This left a pool of 1,642 individuals who met the basic fMRI requirements. From this pool, only participants with available VIQ scores were enrolled in the final analysis. This yielded a final sample of 219 individuals with ASD and 322 HCs.

Group comparisons across sites revealed no significant differences in age or sex distribution between ASD and HCs at most sites ($p > 0.05$), except for the site of Georgetown University (GU) with 14 males and 1 female in the ASD group versus 15 males and 16 females in the HCs ($p = 0.002$). As anticipated, VIQ scores were generally lower in the ASD group, reaching statistical significance at New York University Site 1 (NYU1; $p = 0.003$), University of California, Los Angeles (UCLA; $p = 0.007$), and University of Southern California (USM; $p < 0.001$). Finally, to further account for residual between-site variability, all regression analyses included site as a covariate, thereby ensuring that demographic and cognitive comparisons were not confounded by site-specific effects.

Table 1 Demographic information of patients with ASD and HCs

Cohort name	Participants		Sex			Age(years)			VIQ Scores		
			ASD	HCs		Mean(SD)			Mean(SD)		
	ASD	HCs	M/F	M/F	*p*-value	ASD	HCs	*p*-value	ASD	HCs	*p-value*
Caltech	3	10	3/0	6/4	0.220	25.67(9.81)	27.7(12.20)	0.798	109.33(9.61)	112.70(15.81)	0.738
ETH	6	19	6/0	19/0	-	20.67(4.27)	22.95(4.78)	0.308	110.00(14.41)	114.53(15.52)	0.533
GU	15	31	14/1	15/16	0.002	10.53(1.30)	10.06(1.88)	0.390	118.53(12.37)	119.48(16.12)	0.842
NYU1	59	97	48/11	77/20	0.766	14.88(7.85)	14.62(6.40)	0.820	107.03(17.21)	114.32(13.37)	0.003
Pitt	22	23	19/3	20/3	0.955	18.41(7.14)	18.96(6.66)	0.791	106.91(13.81)	107.09(10.31)	0.961
SDSU	12	21	12/0	16/5	0.070	14.58(1.73)	13.90(1.51)	0.248	113.42(17.75)	106.10(10.31)	0.142
Stanford_1	17	16	14/3	12/4	0.619	9.36(1.58)	9.63(1.70)	0.638	109.59(21.30)	111.62(20.54)	0.782
Stanford_2	17	18	16/1	16/2	0.594	10.47(1.23)	10.50(1.38)	0.948	110.41(16.02)	115.78(16.21)	0.332
Trinity2	13	18	13/0	18/0	-	13.85(3.58)	15.94(2.73)	0.074	115.08(10.86)	119.33(14.32)	0.376
UCLA	13	38	12/1	31/7	0.369	12.38(1.85)	12.24(2.12)	0.824	100.54(14.66)	111.11(10.51)	0.007
UM	3	4	3/0	4/0	-	15.33(0.58)	22.00(5.83)	0.112	107.67(11.06)	112.00(11.40)	0.636
USM	39	27	39/0	27/0	-	22.87(8.43)	20.78(6.62)	0.284	97.54(17.89)	114.22(13.12)	<0.001

Note: The 003 and 004 sites were excluded due to poor normalization, whereas sites 018 were excluded due to the lack of HCs.

Abbreviation: ASD, autism spectrum disorder; HCs, Healthy Controls; VIQ, Verbal IQ; SD, Standard Deviation; M, Male; F, Female; Caltech, California Institute of Technology; ETH, Swiss Federal Institute of Technology Zürich; GU, Georgetown University; NYU1, New York University (Site 1); Pitt, University of Pittsburgh; SDSU, San Diego State University; Stanford_1, Stanford University (Site 1); Stanford_2, Stanford University (Site 2); Trinity2, Trinity College Dublin (Site 2); UCLA, University of California, Los Angeles; UM, University of Michigan; USM, University of Southern California.

3.2. Results of FC

Following the computation of FC, significant alterations were observed in the connectivity of specific connections between brain regions, as illustrated in Figure 1.

Group-level comparisons revealed significant changes in inter-network connectivity. To facilitate interpretation of large-scale FC alterations in ASD, each of the 90 AAL regions was assigned—via its MNI centroid—to one of Yeo et al.'s seven intrinsic functional networks: VN, somatomotor (SMN), DAN, ventral attention (VAN), frontoparietal (FP), limbic, and default-mode (DMN) (Schaefer et al., 2018; Yeo et al., 2011). Yeo's seven-network parcellation was derived from a comprehensive analysis of intrinsic FC MRI in the human cortex and demonstrated serial hierarchical processing in sensory systems as well as topographically specific connectivity in sensory–motor regions (Yeo et al., 2011). ASD patients exhibited widespread increased FC in the DMN, DAN, and FP ($p < 0.05$). Conversely, decreased FC was observed within the DMN, Limbic, SMN, and VN, and between the FP and DMN, FP and Limbic, DMN and Limbic, VN and SMN, and Ventral and DAN ($p < 0.05$).

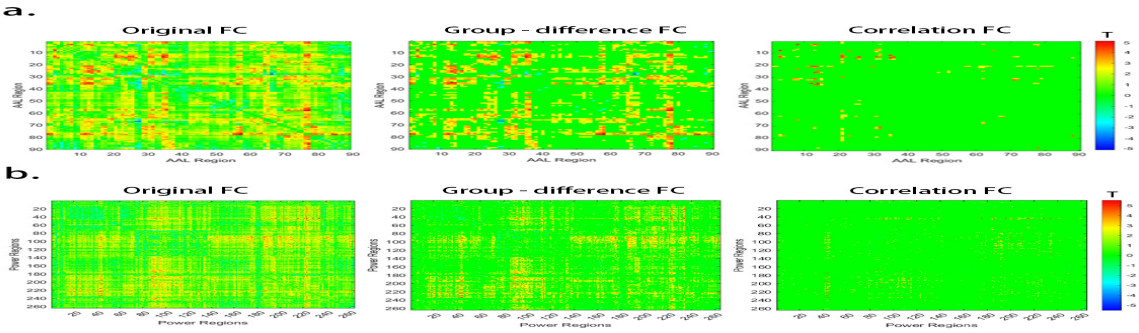

Figure 1 *T*-value heatmaps illustrating the progressive refinement of FC features.

The Original FC matrix shows *T*-values for all pairwise connections across participants, reflecting the overall FC architecture. The Group-difference FC matrix highlights connections that significantly differed between ASD and HCs, as identified by two-sample t-tests with FDR correction ($p < 0.05$). The Correlation FC matrix further refines these group-differentiated connections by retaining only those that were significantly correlated with VIQ scores ($p < 0.05$), thus emphasizing connections that were both diagnosis-sensitive and cognitively relevant.

3.3. Global properties of the functional brain networks

As shown in Figure 2, both the ASD and HCs demonstrated functional networks with small-world properties across the defined sparsity range (0.05–0.5), as evidenced by AUC values for sigma > 1, gamma > 1, and lambda ≈ 1. The AUC of gamma in the ASD group was significantly lower than that in the HCs ($p < 0.05$), indicating reduced local clustering in ASD. However, no significant differences were found in the AUCs of lambda, sigma, Cp, or Lp (all $p > 0.05$), suggesting comparable global integration and small-world topology between groups. Likewise, the AUCs of both Eloc and Eglob did not differ significantly between ASD and HCs ($p > 0.05$).

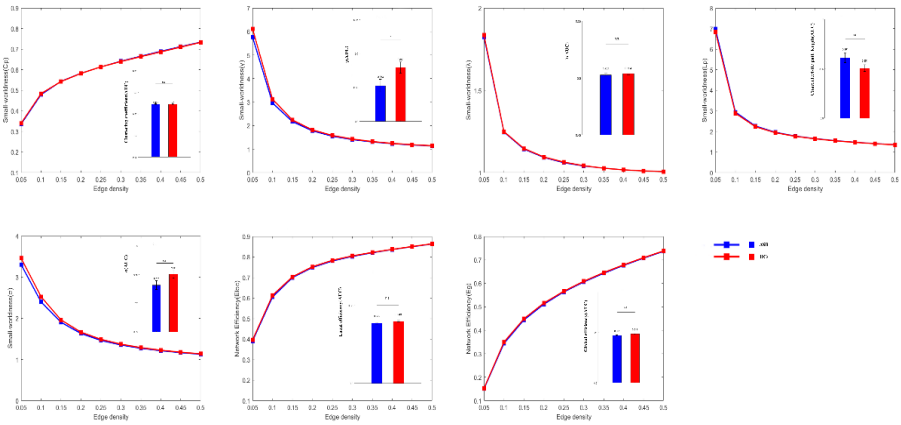

Figure 2 Small-world properties and network efficiency of functional brain networks in ASD and HCs. Functional brain network metrics for individuals with autism spectrum disorder (ASD, labeled as Patient, shown in blue) and healthy controls (HCs, labeled as Control, shown in red). The x-axis of the line charts represents the sparsity range (0.05–0.5), and the lines indicate group-averaged values across this range. The bar charts display the AUC for each metric.

* indicates significant group differences ($p < 0.05$, post hoc t-test, corrected for multiple comparisons); n.s. denotes non-significant differences. HCs: healthy controls; ASD: autism spectrum disorder; AUC: area under the curve.

3.4. Nodal properties of functional brain networks

As shown in Figure 3 and Table 2, several brain regions exhibited significant alterations in DC and NE in ASD patients relative to HCs.

Specifically, ASD patients demonstrated increased DC and NE in the right opercular inferior frontal gyrus (IFGoperc.R), left triangular inferior frontal gyrus (IFGtriang.L), right triangular inferior frontal gyrus (IFGtriang.R), left medial superior frontal gyrus (SFGmed.L), right anterior cingulate gyrus (ACG.R), left anterior cingulate gyrus (ACG.L), left thalamus (THA.L), and right thalamus (THA.R) ($p < 0.05$).

Conversely, compared with HCs, DC was lower in ASD patients in the left superior frontal orbital gyrus (ORBsup.L), left rectus gyrus (REC.L), right rectus gyrus (REC.R), and left fusiform gyrus (FUS.L). Decreased NE was also found in ORBsup.L, left orbital middle frontal gyrus (ORBmid.L), REC.L, REC.R, left parahippocampal gyrus (PHG.L), PHG.R, left amygdala (AMYG.L), right superior occipital gyrus (SOG.R), FUS.L, left superior parietal gyrus (SPG.L), right superior temporal pole (TPSup.R), right middle temporal gyrus (MTG.R), left middle temporal pole (TPMid.L), right middle temporal pole (TPMid.R), left inferior temporal gyrus (ITG.L), and right inferior temporal gyrus (ITG.R) ($p < 0.05$).

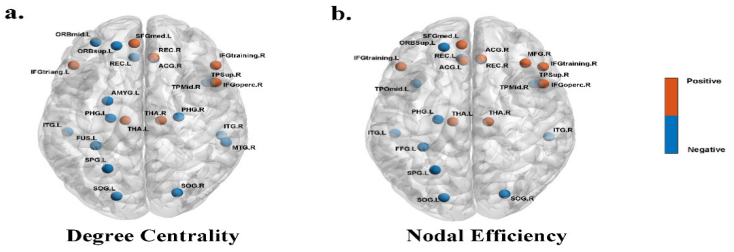

Figure 3 Brain regions with significant differences in the DC (a), and NE (b) between ASD and HCs. The red sphere demonstrated that nodal network properties in the ASD group were increased compared with the HCs.

Table 2 The abnormal node network characteristics displayed between the ASD and HCs.

Brain Regions	Degree Centrality		Nodal Efficiency	
	t Values	*p* Values	*t* Values	*p* Values
ASD > HCs				
IFGoperc.R	2.2781	0.0231	2.1879	0.0291
IFGtriang.L	3.4769	0.0005	2.8878	0.0040
IFGtriang.R	2.3763	0.0178	2.1499	0.0320
SFGmed.L	2.6326	0.0087	2.1526	0.0317
ACG.R	3.2893	0.0011	2.7316	0.0065
ACG.L	2.1284	0.0338		
THA.L	3.8845	0.0001	3.8447	0.0001
THA.R	4.4033	<0.0001	4.2941	<0.0001
ASD < HCs				
ORBsup.L	-2.3820	0.0176	-2.4016	0.0166
ORBmid.L			-2.3932	0.0170
REC.L	-2.6679	0.0078	-3.1486	0.0017
REC.R	-3.3828	0.0007	-3.5156	0.0004
PHG.L	-2.2999	0.0218	-2.8396	0.0046
PHG.R			-2.0941	0.0367
AMYG.L			-2.0796	0.0380
SOG.L	-1.9341	0.0536	-1.9500	0.0516
SOG.R	-2.0096	0.0449	-2.2903	0.0223
FUS.L	-3.5071	0.0004	-3.9215	<0.0001
SPG.L	-1.9278	0.0543	-2.0624	0.0396
TPSup.R	-2.1063	0.0356	-2.3226	0.0205
MTG.R			-2.1945	0.0286
TPMid.L	-2.0562	0.0402		
TPMid.R	-2.8616	0.0043	-2.4384	0.0150
ITG.L	-1.9736	0.0489	-2.2616	0.0241
ITG.R	-2.4471	0.0147	-2.5677	0.0105

Abbreviations: IFGoperc, opercular inferior frontal gyrus; IFGtriang, triangular inferior frontal gyrus; SFGmed, medial superior frontal gyrus; ACG, anterior cingulate gyrus; THA, thalamus; ORBsup, superior frontal orbital gyrus; ORBmid, middle frontal orbital gyrus; REC, gyrus rectus; PHG, parahippocampal gyrus; AMYG, amygdala; SOG, superior occipital gyrus; FUS, fusiform gyrus; SPG, superior parietal gyrus; TPSup, superior temporal pole; MTG, middle temporal gyrus; TPMid, middle temporal pole; ITG, inferior temporal gyrus.

3.5. Correlation between network metrics and VIQ scores

The correlations between VIQ scores and the topological attributes of five key nodes were presented in Figure 4. DC of the bilateral ACG was negatively correlated with VIQ (left ACG: $r = -0.085$, $p < 0.05$; right ACG: $r = -0.098$, $p < 0.05$). In contrast, VIQ scores were positively correlated with DC of the left SOG ($r = 0.107$, $p = 0.013$) and with NE of the bilateral SOG (left SOG: $r = 0.119$, $p = 0.005$; right SOG: $r = 0.083$, $p < 0.05$). No other graph-theoretical metrics nor brain regions showed significant associations with VIQ. Moreover, after correlating FC with VIQ scores, several network pairs exhibited significant negative associations ($p < 0.05$), including connections between the FP and DMN; FP and Limbic networks; DMN and Limbic networks; VN and SMN networks; and DAN and VAN.

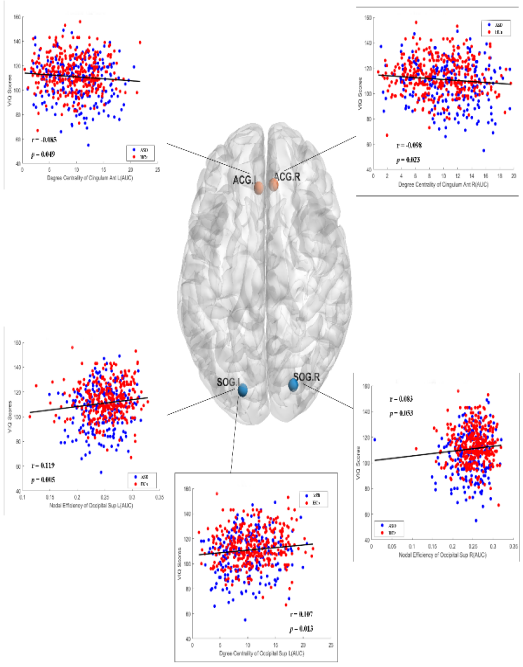

Figure 4 Scatter plots of node attributes versus VIQ scores for both ASD (blue) and HCs (red) groups. ACG, anterior cingulate gyrus; SOG, superior occipital gyrus; L, left; R, right; VIQ, Verbal IQ.

3.6. Classification Accuracy

A summary of classification performance for each feature set and model was presented in Table 3. When using a standard SVM classifier without dimensionality reduction, manual feature selection based on group differences increased the AUC from 0.7143 (Raw feature set) to 0.7336. Incorporating VIQ scores into

the group-difference features further raised the AUC to 0.7451.

When PCA was applied followed by UMAP before SVM classification, the highest AUC (0.7514) was obtained using the Raw feature set. Applying PCA and UMAP to the group-difference features yielded an AUC of 0.7024, and applying PCA and UMAP to the group-difference + VIQ features yielded an AUC of 0.7217. Manifold-based dimensionality reduction on the full feature matrix achieved the best performance and still demonstrated that including VIQ scores improved model discrimination.

Table 3 Area Under the Curve of feature sets and models.

	SVM	PCA_UMAP_SVM
Raw Features	0.7143	**0.7514**
Group-difference Features	0.7336	0.7024
Group-difference_VIQ Features	**0.7451**	0.7217

4. Discussion

In the present study, we examined brain functional alterations associated with language impairment in ASD using FC and network topology and VIQ scale, and also evaluated classification performance using SVM and UMAP manifold learning. There are three main results: (1) ASD patients showed widespread FC alterations, with increased inter-network connectivity among several large-scale networks and decreased intra-network connectivity in regions involved in social and sensory processing; (2) Network metric analyses revealed significant changes of DC and NE in language-related regions ; (3) A baseline SVM required manual feature selection to achieve competitive accuracy, whereas SVM with manifold learning–based dimensionality reduction achieved superior performance using raw features without manual selection. Moreover, including VIQ scores consistently improved classification accuracy, suggesting that VIQ-related network features support the relevance of cognitive-functional alterations in ASD, providing a proof-of-principle for integrating behavioral scales into neuroimaging analysis.

The FC results revealed widespread increased FC across multiple networks in ASD, alongside reduced connectivity within the DMN, limbic, and sensory-motor systems. While Just et al. (Just et al., 2004) reported reduced long-range connectivity in ASD using task-based fMRI during language processing, our findings extend this framework by demonstrating that increased FC and reduced network segregation can coexist with selective long-range connectivity reductions during the resting state. This indicates that disruptions in network integration in ASD may be state-dependent, with the resting brain showing compensatory cross-network increases in connectivity while task-based demands reveal reduced efficiency in global information transfer. Moreover, our findings demonstrated increased local connectivity within the DMN regions as well as within the VN and SMN resting-state networks, consistent with previous reports (Washington et al., 2014; Yerys et al., 2015). However, unlike Yerys et al. (Yerys et al., 2015), who reported decreased connectivity between DMN ROIs and regions within primary sensory, FP, subcortical, and reward networks, our study found reduced connectivity primarily within the DMN, limbic, SMN, and VN, as well as between FP-DMN, FP-limbic, DMN-limbic, VN-SMN, and VAN-DAN. This discrepancy may be due to our larger sample size, indicating that the patterns of hypoconnectivity in ASD might be more localized and network-specific than previously reported. Moreover, the increased VN–SMN connectivity supports the notion that perceptual-motor networks are overintegrated, potentially reflecting reliance on sensory scaffolding during language tasks (Vulchanova et al., 2015). Collectively, these FC results underscore the emergent view that ASD is

characterized not by uniform hypo- or hyperconnectivity but by a misalignment of network segregation and integration that is closely tied to language processing demands.

Graph-theoretical analysis of global network topology demonstrated that both ASD and HCs maintained small-world characteristics ($\sigma > 1$, $\gamma > 1$, $\lambda \approx 1$) across a sparsity range of 0.05-0.5. Specifically, the ASD group exhibited a significant reduction in the normalized γ AUC, indicating a loss of local modularity. These findings align with the theoretical model of optimal segregation–integration balance described by Bullmore and Sporns (Bullmore et al., 2009) and Rubinov and Sporns (Rubinov et al., 2010), in which disruption to γ compromises modular processing, prompting—but failing to fully realize—compensatory global interactions. In contrast, although the characteristic Lp AUC showed an increase in the ASD group, these differences did not reach statistical significance after correction. Moreover, the AUC values for Eloc, λ, Eg, and σ were all lower in the ASD group, but these differences did not reach significance, further implying a subtle decline in overall network integration. Consistent with our results, prior studies (Keown et al., 2017; Peng et al., 2022) have similarly reported declines in σ alongside increases in Lp, suggesting a potential trend toward altered small-world topology in ASD, though our data indicates that local clustering deficits γ emerge as the most robust global network aberration in this multisite sample. This emphasizes that impaired segregation at the module level may be a key feature of ASD network dysfunction, whereas other global integration metrics show only subtle, subthreshold deviations.

At the nodal level, ASD showed a distinct imbalance between hyper- and hypo-connectivity across regions subserving language production, semantic integration, and socio-emotional processing. DC and NE were significantly elevated in bilateral IFGtriang, IFGoperc, SFGmed, ACG, and THA. These areas form part of the executive-language control network and are critical for top-down regulation of speech production, syntactic processing, and attentional modulation (Cristia et al., 2014; Friederici, 2011). Compared to HCs, ASD participants exhibited significantly increased DC in the IFG, ACG, and thalamus, consistent with previous findings of elevated DC in these regions in ASD (Lee et al., 2017), suggesting that hyper-centrality within frontal and limbic circuits may underlie atypical cognitive and affective processing in ASD. In contrast, we also observed decreased DC in temporal regions, including the MTG, ITG, and temporal pole, whereas Lee et al. reported more widespread DC increases across the STG. This difference may reflect their age-stratified approach versus our lifespan sample, indicating that hypoconnectivity in temporal regions may vary with age or individual heterogeneity. Additionally, regions implicated in semantic memory (PHG), emotion regulation (AMYG, REC), and VN recognition (FUS, SOG), along with the orbitofrontal cortex (ORBsup, ORBmid), exhibited reduced centrality and efficiency—echoing previous reports of disrupted fusiform–amygdala coupling in ASD (Kleinhans et al., 2008). These alterations likely impeded integration of emotional and contextual information during language use (Vulchanova et al., 2015), consistent with documented deficits in pragmatic language and context-dependent communication in ASD (Márquez-García et al., 2023). Taken together, the nodal architecture suggests that ASD is characterized by frontally weighted hyperconnectivity compensating for weakened posterior–limbic integration. This imbalance may help explain why individuals with ASD, despite preserved or even enhanced activation in control-related regions, struggle to ground language in contextually and socially appropriate ways—supporting our hypothesis that altered nodal connectivity underlies the heterogeneous language profiles observed in ASD.

Correlation analyses revealed that decreased FC between the FP, DMN, and limbic networks was negatively associated with VIQ, consistent with Redcay et al. (Redcay et al., 2013), who reported that lower DMN connectivity correlated with greater communication difficulties in ASD. At the nodal level, DC of the bilateral ACG was negatively associated with VIQ, whereas DC and NE of the SOG were positively correlat-

ed with VIQ. The negative ACG–VIQ relationship suggested that overcentrality of an emotion- and conflict-monitoring hub may hamper language performance by diverting cognitive resources, in line with Bush et al. (Bush et al., 2000) on ACG's role in attentional control and emotion regulation. In contrast, enhanced SOG connectivity appears to support visual-based scaffolding of verbal processes, corroborating Vulchanova et al.'s (Vulchanova et al., 2015) notion of augmented reliance on contextual visual cues. These associations confirm Johnson et al.'s (Johnson et al., 2021) assertion that VIQ reflects underlying network integrity and highlight the value of combining neurofunctional and psychometric measures to capture the cognitive heterogeneity of ASD. No other nodal or global metrics show significant VIQ correlations, indicating that ACG and SOG serve as principal neural substrates linking network topology to verbal ability.

For the machine learning results, using SVM with the selected differential features combined with VIQ achieved modest performance, reaching an AUC of approximately 0.7451. The PCA+UMAP approach was able to achieve an AUC of approximately 0.7514 using only the raw features from each group. These AUC values are broadly in line with existing ABIDE classification studies, suggesting that while the classifier captures meaningful patterns, it functions primarily as a proof-of-principle analysis rather than a clinically ready diagnostic tool. Both methods found that the incorporation of VIQ-related metrics further improved performance by 1–2%, suggesting that VIQ may provide additional discriminative information beyond connectivity patterns alone. These results reinforce Pereira et al.'s (Pereira et al., 2009) demonstration of SVM's sensitivity to high-dimensional neuroimaging features and extend Casanova et al.'s (Casanova et al., 2021) finding that manifold learning uncovers intrinsic data structure to enhance classification. Notably, automatic dimensionality reduction uncovers discriminative information while preserving intrinsic data structure. The consistent performance gain from integrating VIQ underscores Lin et al.'s (Lin et al., 2024) call for multimodal biomarkers. Overall, our machine learning analysis illustrates that low-dimensional embeddings, combined with behavioral indices, constitute a useful analytical strategy for exploring ASD phenotype stratification, even if current classification accuracies remain below the threshold for clinical utility.

Despite these findings, this study has several limitations. The cross-sectional design limited our ability to characterize longitudinal changes in network topology and verbal functioning, and future studies with follow-up assessments are needed to clarify causal relationships and developmental trajectories. Although the multisite sample increased statistical power, heterogeneity in scanner hardware, acquisition parameters, and recruitment strategies may have introduced additional noise; we only applied linear regression to control for site effects, and future work could benefit from stricter acquisition protocols or advanced harmonization approaches. In addition, our preprocessing pipeline did not include volume scrubbing or censoring of high-motion time points, which may have biased functional connectivity and graph-theoretical estimates and should therefore be considered a limitation. Furthermore, VIQ was employed as a proxy measure of verbal abilities rather than a comprehensive index of language function. While VIQ captures certain aspects of verbal reasoning, it does not fully reflect pragmatic language use or real-world communicative competence. Finally, although UMAP-based dimensionality reduction modestly improved classification performance, the resulting low-dimensional embeddings lack direct neurobiological interpretability, warranting more transparent modeling and feature-level analyses in future studies.

5. Conclusion

In summary, patients with ASD exhibited dysregulated functional connections across multiple brain

networks and regions, and these alterations were significantly associated with verbal IQ. While global network analysis revealed significant alterations specifically in normalized clustering, other small-world metrics showed only non-significant trends, suggesting a localized rather than a broad disruption of topology. Both manual feature sets augmented with VIQ and automated PCA + UMAP embedding of raw connectivity measures combined with VIQ achieved modest but competitive discrimination between ASD and HCs, consistent with results from other large-scale multisite datasets. These results provide a neuroscientific foundation for understanding language-related network alterations in ASD and serve as a proof-of-principle for the relevance of VIQ-related features.

Funding

This study was funded by the National Natural Science Foundation of China (82374578), in collaboration with the First Affiliated Hospital of Tianjin University of Traditional Chinese Medicine, under the project titled "External Manifestations and Internal Mechanisms of 'Effective Qi Arrival' in Tongguan Liqiao Acupuncture". This work was also supported by the Open Project of the Heilongjiang Provincial Key Laboratory of Autonomous Intelligence and Information Processing, under the project "Research on Real-Time Target Recognition Methods for UAV Images Based on Deep Reinforcement Learning" (Project No. ZZXC202303).

CRediT authorship contribution statement

Xize Jia, Huibin Ma, and Jinying Wu conceived and designed this study. Lulu Cheng, Linlin Zhan and Zeqi Hao compiled the ABIDE database. Jinying Wu executed the data analysis and wrote the first manuscript. Lanfen Chen, Jiaying Song and Hang Zhang helped coordinate the study and revised the manuscript. All authors have made significant scientific contributions to this article and reviewed the article.

Acknowledgments

We thank the Hangzhou NaoHai Technology Laboratory(https://www.brainimaging.cn) for the technical support provided by its scientific research platform in this study.

Declaration of competing interest

The authors declared that this research has no financial conflicts of interest.

Data availability statement

The data used in this study were obtained from the Autism Brain Imaging Data Exchange (http://fcon_1000.projects.nitrc.org/indi/abide/) public database.

Ethics approval statement

All procedures performed were following the ethical standards of the appropriate institutional research boards and with the 1964 Helsinki declaration and its later amendments or comparable ethical standards.

References

[1] Achard, S., et al. (2007). Efficiency and Cost of Economical Brain Functional Networks. *PLOS Computational Biology, 3*(2), e17. doi:10.1371/journal.pcbi.0030017

[2] Alaerts, K., et al. (2015). Functional Organization of the Action Observation Network in Autism: A Graph Theory Approach. PLoS One, 10(8), e0137020. doi:10.1371/journal.pone.0137020

[3] Alamdari, S. B., et al. (2022). Cognitive theories of autism based on the interactions between brain functional networks. Front Hum Neurosci, 16, 828985. doi:10.3389/fnhum.2022.828985

[4] Association, A. P. (2013). *Diagnostic and statistical manual of mental disorders: DSM-5*. Washington, DC: American psychiatric association.

[5] Benjamini, Y., et al. (1995). Controlling the false discovery rate: a practical and powerful approach to multiple testing. Journal of the Royal Statistical Society: Series B (Methodological), 57(1), 289-300.

[6] Bi, X. A., et al. (2018). Classification of Autism Spectrum Disorder Using Random Support Vector Machine Cluster. Front Genet, 9, 18. doi:10.3389/fgene.2018.00018

[7] Bi, X. A., et al. (2018). Abnormal Functional Connectivity of Resting State Network Detection Based on Linear ICA Analysis in Autism Spectrum Disorder. Front Physiol, 9, 475. doi:10.3389/fphys.2018.00475

[8] Bressler, S. L., et al. (2010). Large-scale brain networks in cognition: emerging methods and principles. Trends Cogn Sci, 14(6), 277-290. doi:10.1016/j.tics.2010.04.004

[9] Bullmore, E., et al. (2009). Complex brain networks: graph theoretical analysis of structural and functional systems. Nat Rev Neurosci, 10(3), 186-198. doi:10.1038/nrn2575

[10] Bush, G., et al. (2000). Cognitive and emotional influences in anterior cingulate cortex. Trends Cogn Sci, 4(6), 215-222. doi:10.1016/s1364-6613(00)01483-2

[11] Casanova, R., et al. (2021). Embedding Functional Brain Networks in Low Dimensional Spaces Using Manifold Learning Techniques. Front Neuroinform, 15, 740143. doi:10.3389/fninf.2021.740143

[12] Chen, L., et al. (2021). Changes in the topological organization of the default mode network in autism spectrum disorder. Brain Imaging Behav, 15(2), 1058-1067. doi:10.1007/s11682-020-00312-8

[13] Cristia, A., et al. (2014). Predicting individual variation in language from infant speech perception measures. Child Dev, 85(4), 1330-1345. doi:10.1111/cdev.12193

[14] Dai, Z., et al. (2012). Discriminative analysis of early Alzheimer's disease using multi-modal imaging and multi-level characterization with multi-classifier (M3). NeuroImage, 59(3), 2187-2195. doi:10.1016/j.neuroimage.2011.10.003

[15] Di Martino, A., et al. (2017). Enhancing studies of the connectome in autism using the autism brain imaging data exchange II. Sci Data, 4, 170010. doi:10.1038/sdata.2017.10

[16] Di Martino, A., et al. (2014). The autism brain imaging data exchange: towards a large-scale evaluation of the intrinsic brain architecture in autism. Mol Psychiatry, 19(6), 659-667. doi:10.1038/mp.2013.78

[17] Dichter, G. S. (2012). Functional magnetic resonance imaging of autism spectrum disorders. Dialogues Clin Neurosci, 14(3), 319-351. doi:10.31887/DCNS.2012.14.3/gdichter

[18] Freeman, L. C. (1978). Centrality in social networks conceptual clarification. Social Networks, 1(3), 215-239. doi:https://doi.org/10.1016/0378-8733(78)90021-7

[19] Friederici, A. D. (2011). The brain basis of language processing: from structure to function. Physiol Rev, 91(4), 1357-1392. doi:10.1152/physrev.00006.2011

[20] Friston, K. J., et al. (1996). Movement-related effects in fMRI time-series. Magnetic Resonance in Medicine, 35(3), 346-355. doi:10.1002/mrm.1910350312

[21] Gibson, J., et al. (2013). Social communication disorder outside autism? A diagnostic classification approach to delineating pragmatic language impairment, high functioning autism and specific language impairment. J Child Psychol Psychiatry, 54(11), 1186-1197. doi:10.1111/jcpp.12079

[22] Goense, J., et al. (2016). fMRI at High Spatial Resolution: Implications for BOLD-Models. Front Comput

Neurosci, 10, 66. doi:10.3389/fncom.2016.00066

[23] Healy, J., et al. (2024). Uniform manifold approximation and projection. Nature Reviews Methods Primers, 4(1), 82. doi:10.1038/s43586-024-00363-x

[24] Horien, C., et al. (2022). Functional Connectome-Based Predictive Modeling in Autism. Biol Psychiatry, 92(8), 626-642. doi:10.1016/j.biopsych.2022.04.008

[25] Jia, X.-Z., et al. (2019). RESTplus: an improved toolkit for resting-state functional magnetic resonance imaging data processing. Science Bulletin, 64. doi:10.1016/j.scib.2019.05.008

[26] Johnson, C. N., et al. (2021). Cognitive correlates of autism spectrum disorder symptoms. Autism Res, 14(11), 2405-2411. doi:10.1002/aur.2577

[27] Just, M. A., et al. (2004). Cortical activation and synchronization during sentence comprehension in high-functioning autism: evidence of underconnectivity. Brain, 127(Pt 8), 1811-1821. doi:10.1093/brain/awh199

[28] Keown, C. L., et al. (2017). Network organization is globally atypical in autism: A graph theory study of intrinsic functional connectivity. Biol Psychiatry Cogn Neurosci Neuroimaging, 2(1), 66-75. doi:10.1016/j.bpsc.2016.07.008

[29] Kjelgaard, M. M., et al. (2001). An Investigation of Language Impairment in Autism: Implications for Genetic Subgroups. Lang Cogn Process, 16(2-3), 287-308. doi:10.1080/01690960042000058

[30] Kleinhans, N. M., et al. (2008). Abnormal functional connectivity in autism spectrum disorders during face processing. Brain, 131(Pt 4), 1000-1012. doi:10.1093/brain/awm334

[31] Klöppel, S., et al. (2012). Diagnostic neuroimaging across diseases. *NeuroImage, 61*(2), 457-463. doi:10.1016/j.neuroimage.2011.11.002

[32] Larson, C., et al. (2022). Structural language impairment in Autism Spectrum Disorder versus Loss of Autism Diagnosis: Behavioral and neural characteristics. Neuroimage Clin, 34, 103043. doi:10.1016/j.nicl.2022.103043

[33] Lee, Y., et al. (2017). Autism Spectrum Disorder Related Functional Connectivity Changes in the Language Network in Children, Adolescents and Adults. Front Hum Neurosci, 11, 418. doi:10.3389/fnhum.2017.00418

[34] Li, W., et al. (2023). The reconfiguration pattern of individual brain metabolic connectome for Parkinson's disease identification. MedComm (2020), 4(4), e305. doi:10.1002/mco2.305

[35] Li, W., et al. (2017). Remodeling Pearson's Correlation for Functional Brain Network Estimation and Autism Spectrum Disorder Identification. Front Neuroinform, 11, 55. doi:10.3389/fninf.2017.00055

[36] Li, W., et al. (2020). Functional connectivity network estimation with an inter-similarity prior for mild cognitive impairment classification. Aging (Albany NY), 12(17), 17328-17342. doi:10.18632/aging.103719

[37] Lin, Q., et al. (2024). Functional brain network alterations in the co-occurrence of autism spectrum disorder and attention deficit hyperactivity disorder. Eur Child Adolesc Psychiatry, 33(2), 369-380. doi:10.1007/s00787-023-02165-0

[38] Márquez-García, A. V., et al. (2023). Atypical Associations between Functional Connectivity during Pragmatic and Semantic Language Processing and Cognitive Abilities in Children with Autism. *Brain Sci, 13*(10). doi:10.3390/brainsci13101448

[39] Moraglia, L. E., et al. (2025). Brain Morphometry in Infants Later Diagnosed With Autism is Related to Later Language Skills. Hum Brain Mapp, 46(7), e70221. doi:10.1002/hbm.70221

[40] Orrù, G., et al. (2012). Using Support Vector Machine to identify imaging biomarkers of neurological

and psychiatric disease: a critical review. Neurosci Biobehav Rev, 36(4), 1140-1152. doi:10.1016/j.neubiorev.2012.01.004

[41] Peng, L., et al. (2022). The Altered Pattern of the Functional Connectome Related to Pathological Biomarkers in Individuals for Autism Spectrum Disorder Identification. Front Neurosci, 16, 913377. doi:10.3389/fnins.2022.913377

[42] Pereira, F., et al. (2009). Machine learning classifiers and fMRI: A tutorial overview. NeuroImage, 45(1, Supplement 1), S199-S209. doi:https://doi.org/10.1016/j.neuroimage.2008.11.007

[43] Redcay, E., et al. (2013). Intrinsic functional network organization in high-functioning adolescents with autism spectrum disorder. Front Hum Neurosci, 7, 573. doi:10.3389/fnhum.2013.00573

[44] Riches, N. G., et al. (2010). Sentence repetition in adolescents with specific language impairments and autism: an investigation of complex syntax. Int J Lang Commun Disord, 45(1), 47-60. doi:10.3109/13682820802647676

[45] Rubinov, M., et al. (2010). Complex network measures of brain connectivity: Uses and interpretations. NeuroImage, 52(3), 1059-1069. doi:https://doi.org/10.1016/j.neuroimage.2009.10.003

[46] Rudie, J. D., et al. (2012). Altered functional and structural brain network organization in autism. Neuroimage Clin, 2, 79-94. doi:10.1016/j.nicl.2012.11.006

[47] Schaefer, A., et al. (2018). Local-Global Parcellation of the Human Cerebral Cortex from Intrinsic Functional Connectivity MRI. Cereb Cortex, 28(9), 3095-3114. doi:10.1093/cercor/bhx179

[48] Sporns, O. (2010). Networks of the Brain. Cambridge, MA: The MIT Press.

[49] Sporns, O. (2013). Structure and function of complex brain networks. Dialogues Clin Neurosci, 15(3), 247-262. doi:10.31887/DCNS.2013.15.3/osporns

[50] Thomas, C. G., et al. (2002). Noise reduction in BOLD-based fMRI using component analysis. NeuroImage, 17(3), 1521-1537. doi:10.1006/nimg.2002.1200

[51] Tzourio-Mazoyer, N., et al. (2002). Automated Anatomical Labeling of Activations in SPM Using a Macroscopic Anatomical Parcellation of the MNI MRI Single-Subject Brain. NeuroImage, 15(1), 273-289. doi:https://doi.org/10.1006/nimg.2001.0978

[52] van den Heuvel, M. P., et al. (2010). Exploring the brain network: a review on resting-state fMRI functional connectivity. Eur Neuropsychopharmacol, 20(8), 519-534. doi:10.1016/j.euroneuro.2010.03.008

[53] Vulchanova, M., et al. (2015). Figurative language processing in atypical populations: the ASD perspective. *Fr*ont Hum Neurosci, 9, 24. doi:10.3389/fnhum.2015.00024

[54] Wang, J., et al. (2015). GRETNA: a graph theoretical network analysis toolbox for imaging connectomics. Front Hum Neurosci, 9, 386. doi:10.3389/fnhum.2015.00386

[55] Washington, S. D., et al. (2014). Dysmaturation of the default mode network in autism. Hum Brain Mapp, 35(4), 1284-1296. doi:10.1002/hbm.22252

[56] Watts, D. J., et al. (1998). Collective dynamics of 'small-world' networks. Nature, 393(6684), 440-442. doi:10.1038/30918

[57] Wechsler, D. (1999). Wechsler abbreviated scale of intelligence. New York: The Psychological Corporation, Harcourt Brace & Company.

[58] Wee, C. Y., et al. (2012). Identification of MCI individuals using structural and functional connectivity networks. NeuroImage, 59(3), 2045-2056. doi:10.1016/j.neuroimage.2011.10.015

[59] Williams, D. L., et al. (2013). Brain function differences in language processing in children and adults with autism. Autism Res, 6(4), 288-302. doi:10.1002/aur.1291

[60] Wu, Y., et al. (2025). Atypical Developmental Patterns of Sensorimotor-Related Networks in Autism Spectrum Disorder: A BrainAGE Study Based on Resting-State fMRI. Autism Res, 18(4), 765-773. doi:10.1002/aur.70008

[61] Yeo, B. T., et al. (2011). The organization of the human cerebral cortex estimated by intrinsic functional connectivity. J Neurophysiol, 106(3), 1125-1165. doi:10.1152/jn.00338.2011

[62] Yerys, B. E., et al. (2015). Default mode network segregation and social deficits in autism spectrum disorder: Evidence from non-medicated children. Neuroimage Clin, 9, 223-232. doi:10.1016/j.nicl.2015.07.018

[63] Zeng, L. L., et al. (2012). Identifying major depression using whole-brain functional connectivity: a multivariate pattern analysis. Brain, 135(Pt 5), 1498-1507. doi:10.1093/brain/aws059

[64] Zhang, J., et al. (2011). Disrupted Brain Connectivity Networks in Drug-Naive, First-Episode Major Depressive Disorder. Biological Psychiatry, 70(4), 334-342. doi:10.1016/j.biopsych.2011.05.018